Journal of Marine Research, 53, 151–169, 1995

Observations of the influence of diurnal convection on upper ocean dissolved gas measurements

by Craig L. McNeil[1,2] and David M. Farmer[1]

ABSTRACT

An important example of the interaction between biological productivity and near-surface oceanography is the role of nocturnal convection and diurnal restratification in modifying the environment in which photosynthetic activity takes place. *In situ* time series measurements of dissolved oxygen reveal the effects of photosynthetic activity, respiration and redistribution by mixing. Moored thermistor time series and frequent CTD casts show that restratification during the day is confined to a warmer shallow surface layer where most of the biological production is expected to occur. The depth and rate of mixing is measured with neutrally buoyant floats which track the vertical excursions of convecting water parcels. Early in the evening, at the onset of night time convection, this warm oxygenated water is mixed down and diluted by deeper less oxygenated water. The interpretation of oxygen time series at specified depths (here 21 m and 30 m) requires knowledge of this mixing process. Use is made of *in situ* dissolved nitrogen time series to infer that gas transfer at the surface is of secondary importance in determining the diurnal dissolved oxygen budget. A qualitative coupled biological/oceanographic model of the data is presented and discussed. It is concluded that a serious overestimate of daily oxygen production can result from excluding diurnal convection from the interpretation of oxygen time series.

1. Introduction

Primary production in the ocean is forced at various time scales primarily by meteorological and oceanographic changes. Of particular interest is the coupling of these driving forces, and the subsequent feedback on primary productivity. It is commonly accepted that the depth of the mean seasonal thermocline increases during colder winter months and shallows during the warmer summer months allowing spring blooms of phytoplankton to occur. Perhaps not fully appreciated however, is the often significant diurnal variability that can exist in meteorological and oceanographic forcing of production. The mixing layer associated with nocturnal convection and daytime solar heating, particularly during winter months, can deepen from the near surface to the base of the seasonal thermocline in a matter of hours.

1. Institute of Ocean Sciences, 9860 West Saanich Road, P.O. Box 6000, Sidney, B.C., Canada, V8L 4B2.
2. Department of Physics and Astronomy, University of Victoria, Victoria, B.C., Canada, V8L 2Y2.

Such changes in mixed layer depth and the vertical motion of convecting water parcels have important implications for biological cycles and primary production.

Other investigators have studied the influence of diurnal convective mixing on, for example, timing of the spring phytoplankton bloom (e.g., Wood and Onken, 1982; Taylor and Stephens, 1993; Stramska and Dickey, 1993) and Patterson (1991) modelled the effect of Langmuir circulation on the photosynthetic response of phytoplankton. However, simultaneous physical and biological measurements have been lacking. The present study makes use of a comprehensive data set including direct observations of the key oceanographic and meteorological variables influencing production, simultaneously with measurements of dissolved oxygen and nitrogen. These data allow an understanding of the physical and biological interactions and also have implications for interpreting measurements of production at sea.

Measurements of primary productivity in the ocean can be made either *in situ* or *in vitro* (Kennish, 1989). Isolation of the water mass during *in vitro* experiments introduces containment effects, which may interfere with the measurement. Comparative studies have been performed to assess the importance of these effects (e.g., Fahnenstiel and Carrick, 1988; Oudot, 1989), with the general conclusion that they can differ by a factor of two or more. In addition to explanations offered by these authors, we suggest that there are other oceanographic processes like nocturnal convection that can lead to the observed disparity. Robertson *et al.* (1993) estimated *in situ* production from measurements of O_2 and pCO_2 from surface water obtained from a ship intake pump. However, an arbitrary definition of mixed layer depth (> 20 m°C from the surface) was imposed when interpreting CTD observations. As will be evident from our observations, caution must be used when interpreting CTD observations to assess mixing layer depths, particularly when the water column is close to being neutrally stable, as is often true during periods of strong diurnal convection.

2. Observations

Our observations were obtained in open ocean conditions off the coast of British Columbia in the vicinity of 48°40′ N and 127°30′ W from February 15 to March 2, 1993. The instrument array consisted of a freely floating surface meteorological buoy, below which were suspended thermistor chains starting at 10 m and extending to 120 m with 5 m vertical resolution. Dissolved oxygen sensors were placed at 21 m and 30 m depth. An additional device measuring gas tension was placed at 40 m depth. Frequent CTD casts were made (every 3 hr) in the vicinity of the instrument array (< 13 km away). The instrument array drifted approximately 4 km per day (~ 5 cm s^{-1}) to the northwest. Spatial variability, which is a complicating factor in nearly all such open-ocean experiments, was minimized in the present study by using a freely floating instrument array designed to drift with the surface currents; thus effects of horizontal variability advecting past the array are minimized. We analyze a

section of dissolved gas time series when the observed wind speed was minimum and the near-surface oceanography was dominated by a diurnal cycle of daytime solar heating and nocturnal convection. McNeil *et al.* (1994) discuss the separation of dissolved nitrogen from measurements of gas tension and oxygen for the same data set. The method requires removal of the dissolved oxygen partial pressure, which is separately measured with dissolved oxygen probes, from the gas tension measurement. The residual partial pressure is mainly that of dissolved nitrogen. Henry's law relates dissolved gas partial pressures to concentrations in the water. Estimated errors for the dissolved nitrogen concentration are 0.7%.

Meteorological and dissolved gas variability for this 5-day time period are shown in Figure 1. Wind speed at 3 m height (Fig. 1a) and air/sea temperature difference (Fig. 1b) were recorded by the surface meteorological buoy. Solar radiation intensity was measured by a meteorological station on the ship (Fig. 1c). The dissolved oxygen at 30 m depth and inferred dissolved nitrogen saturation levels are shown in Figure 1d. Pulsed dissolved oxygen sensors of ENDECO/YSI Inc. (Marion, Massachusetts, USA) were used. Daily bottle samples, taken close to the array, were analyzed for dissolved oxygen content by the Winkler titration method and used to maintain the calibration of the dissolved oxygen probe. A linear fit of: $-0.015\ \text{ml.l}^{-1} \cdot \text{day}^{-1} + 0.451\ \text{ml.l}^{-1}$, was applied to the raw oxygen probe measurements at 30 m to match them to the dissolved oxygen concentrations determined from the *in situ* water samples (see points on Fig. 1d). This is a standard field calibration procedure applicable to dissolved oxygen probe measurements which tend to exhibit a calibration drift with time.

The oxygen record at 30 m shows a clear diurnal signal; within the accuracy of the extraction method, the nitrogen record changes little with time. The stability of the nitrogen signal is mainly attributable to the biological inactivity of dissolved nitrogen gas. The oxygen minimum occurs around noon and the oxygen maximum just before midnight. Oudot (1989) and Robertson *et al.* (1993) similarly observed an oxygen maximum late in the evening, but did not comment on its timing. We believe that this counter-intuitive timing of the oxygen maximum and minimum observed in our data is a consequence of the interaction between convection, photosynthetic activity and respiration as discussed subsequently. The fact that dissolved oxygen is undersaturated and dissolved nitrogen slightly supersaturated, indicates that net respiration of dissolved oxygen has occurred, presumably over the winter months. This is not atypical of open ocean water columns in late winter. We have no other supporting biological measurements to determine whether we observed an initial spring bloom, however a small net mixed layer dissolved oxygen concentration increase of $\sim 0.025\ \text{ml.l}^{-1}$ was observed during this 5-day time period. Such an increase is apparent in Figure 2, where both raw and (1 hr) filtered dissolved oxygen time series measurements are shown. Increases of oxygen saturation level due to increased mixed layer oxygen concentration are compensated by a mixed layer temperature

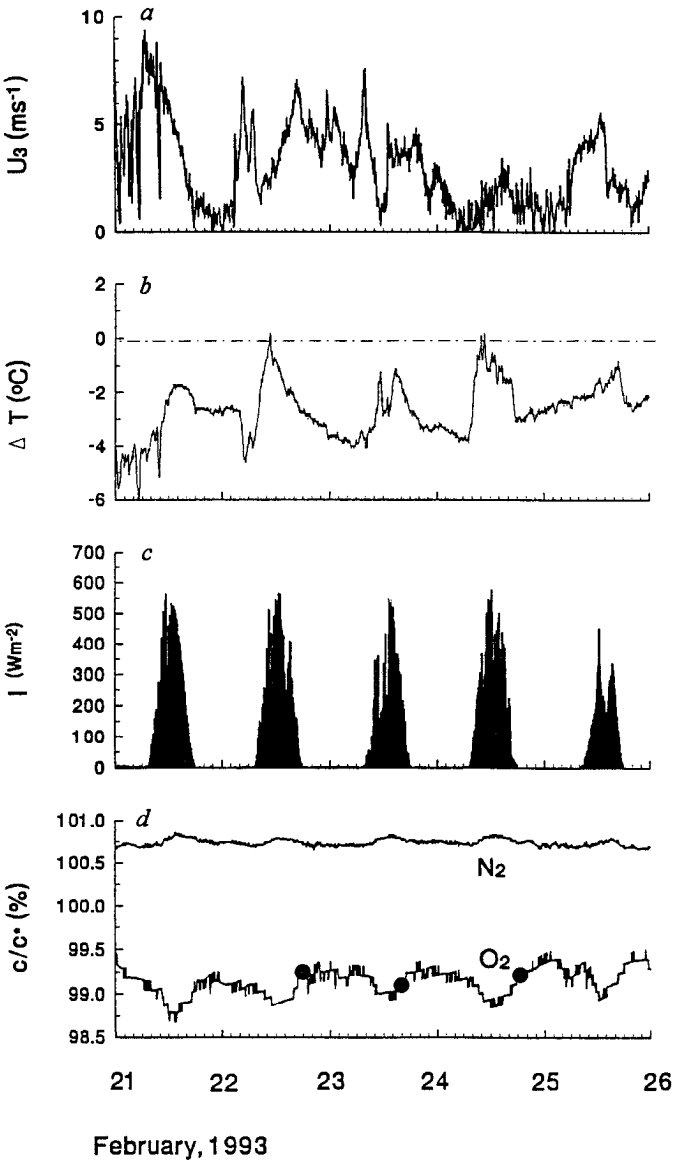

Figure 1. Meteorological and dissolved gas measurements, showing: (a) wind speed at 3 m recorded at a surface buoy; (b) air-sea temperature difference; (c) solar radiation intensity recorded by a ship mounted station; and (d) dissolved oxygen percent saturation level at 30 m depth, and inferred dissolved nitrogen percent saturation level (McNeil *et al.,* 1994). Saturation levels are expressed wrt 1 atmosphere of moist air. *In situ* bottle samples, analyzed for dissolved oxygen concentration by the Winkler titration method (●), were used for correcting a linear drift in the dissolved oxygen time series.

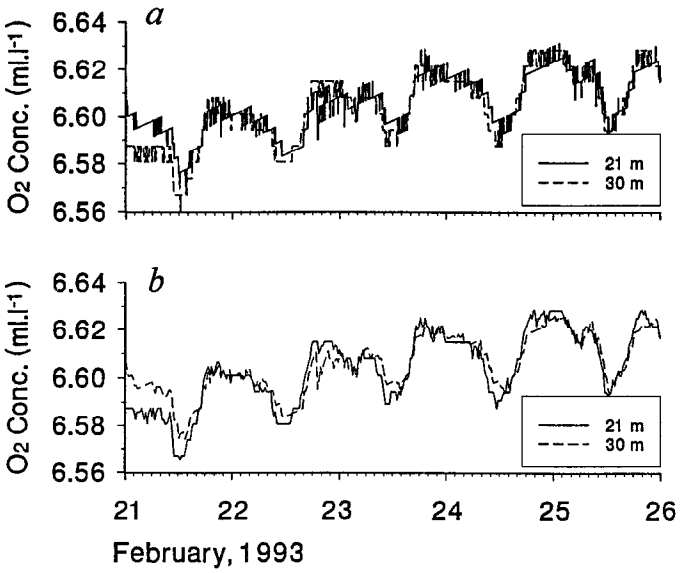

Figure 2. Dissolved oxygen time series at 21 m and 30 m depth, showing: (a) the raw data and (b) the data filtered by a 1 hr average.

decrease, thus maintaining a nearly constant oxygen saturation level (Fig. 1d). Horizontal gradients of oxygen were not measured, hence advective fluxes over the 5-day period are unknown; therefore the rise in oxygen concentration cannot be unambiguously attributed to net oxygen production alone. Figure 2b shows that oxygen changes at 30 m consistently lag the 21 m record by 1–2 hours. The amplitude of the diurnal variation at 21 m consistently exceeds that at 30 m. The phase lags are *not* a consequence of timing errors between the two instruments. This was verified by comparing water temperature records from the thermistor chains at the sensor depths and the water temperature recorded by the dissolved oxygen sensors (being autonomous instruments), and by cross-checking with the deployment and recovery timing.

Respiration and production are not the only mechanisms responsible for dissolved oxygen saturation level variations. Wind induced bubble injection, which tends to supersaturate the water in dissolved gases (Farmer *et al.*, 1993), and seasonal water column temperature changes are important processes in determining longer time scale dissolved gas saturation level changes. The relative biological inactivity of dissolved gaseous nitrogen compared to oxygen provides a differential measurement of biological activity that can be used to separate physical from biological processes affecting oxygen saturation levels. Our time series measurements are not long enough to determine whether the supersaturation of dissolved nitrogen is due to solubility changes of the water column or bubble injection processes.

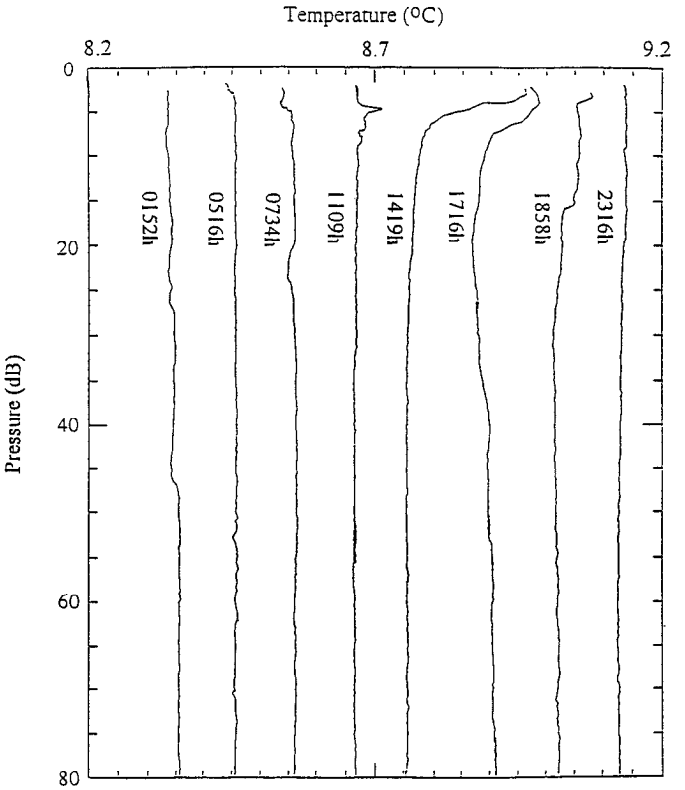

Figure 3. A series of temperature profiles measured on 24 February, 1993 with a Sea-Bird Electronics CTD (temperature offset between each cast is 0.1°C).

During the evening the ocean surface cooled rapidly. This resulted in convection of the upper ocean, the consequences of which are indicated in the sequence of temperature profiles (Fig. 3) from a CTD for a representative day (24 February). There is considerable scatter in the data. This is due in part to the different locations of the casts and the changing meteorological conditions, however the daily convective signature is apparent. Thermistor chain data (Fig. 4) typically show the same signature, although the shallowest thermistor was at 10 m depth. The daily convective cycle is most clearly revealed by unique measurements made in conjunction with E. D'Asaro and G. Dairiki of the University of Washington, using Lagrangian mixed layer floats, ballasted to be very slightly positively buoyant. A composite plot of the float trajectories *versus* time for the period of interest is shown in Figure 5c. Figure 5a shows composite plots of surface solar radiation intensity and dissolved oxygen saturation level at 30 m depth (Fig. 5b). The floats (Fig. 5c) track the convective plumes to the depth of the seasonal thermocline just after midnight, retreating to the near surface during the day. This is consistent with the observations of Brainerd and

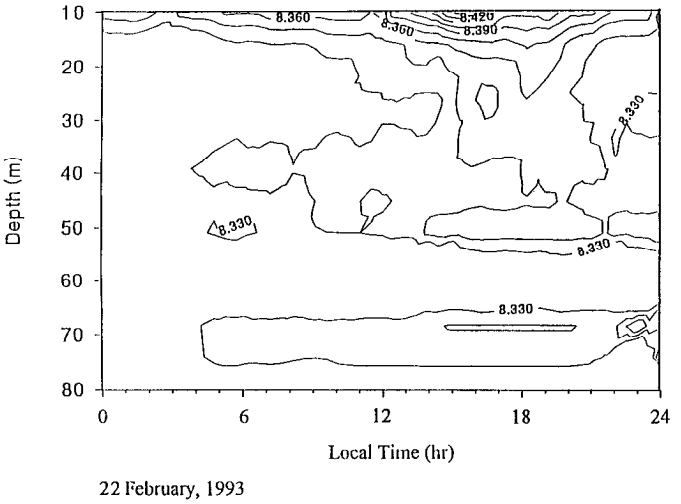

Figure 4. A contour plot of thermistor chain temperature data on 22 February, 1993, showing the isolation of a thermally stratified near-surface layer, which is mixed down in the early evening.

Gregg (1993) who observed increased turbulent kinetic energy, ϵ, throughout the mixed layer in the evening, but decaying levels of ϵ trapped beneath a shallow thermally stratified layer during the day.

Figure 6 shows the effect of convection and restratification on the oxygen and temperature field. We will return to this figure in the comparison of data with model results.

3. Modelling

a. Introduction. Our modelling efforts are primarily motivated by the observations of a periodic dissolved oxygen signal at 21 m and 30 m depth showing a maximum late in the evening and a minimum late in the morning with a noticeable time delay between the time series. After consideration of the supporting data, a simple one dimensional, nondiffusive, mixed layer model coupled with primary production and respiration was chosen. Since our goal is not to simulate the full complexity of the natural phenomenon, but rather to identify certain key features of the physical-biological interactions, we have made use of the simplest possible representations of biological processes affecting dissolved oxygen concentration and the oceanographic changes that occur on a daily basis. The float data are used to identify the convective layer depth, which is taken as the mixed layer thickness in our model. The simplicity of the model assumptions introduces certain limitations to the model. These limitations are indicated in the model development and will be discussed further when comparing the model results with the data.

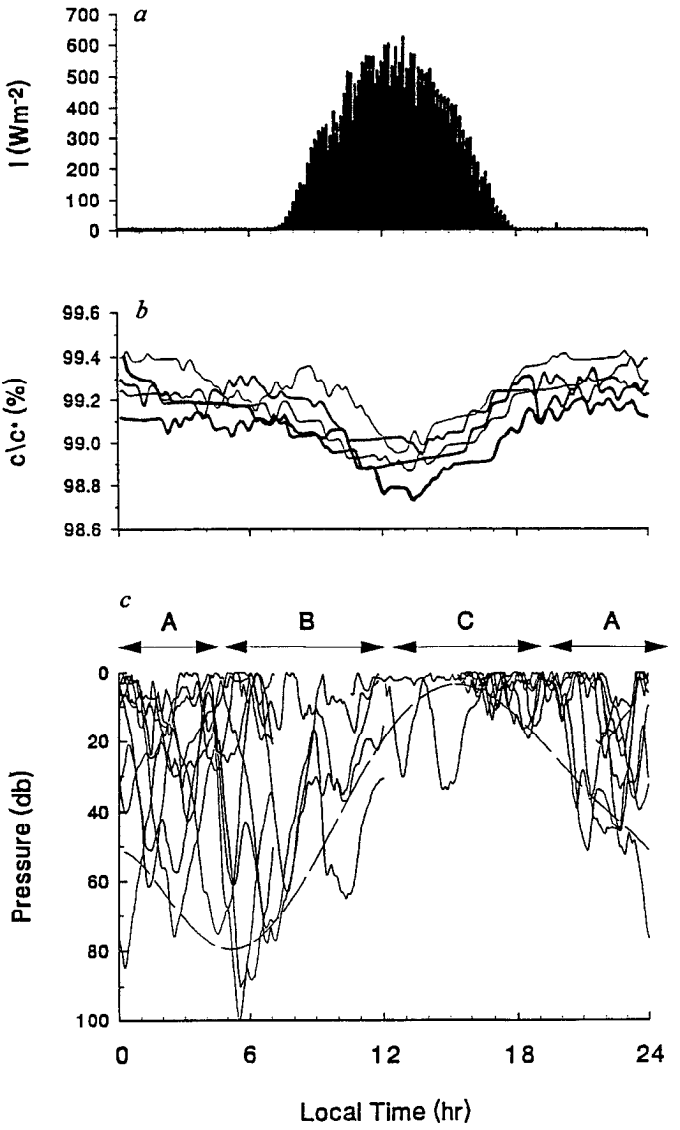

Figure 5. Composite plots of superimposed daily observations from February 21–26, 1993 of: (a) solar radiation intensity; (b) smoothed dissolved oxygen percent saturation level at 30 m depth (Figure 1d); (c) trajectories of neutrally buoyant floats in the mixed layer (courtesy of E. D'Asaro and G. Dairiki). Dominant oceanographic changes occurring during the labelled time periods of the diurnal cycle are: (A) penetrating convection to the base of the seasonal thermocline; (B) inhibition of the mixing depth and subsequent re-stratification; (C) isolation of a thermally stratified surface layer by solar radiation input (see (a) above).

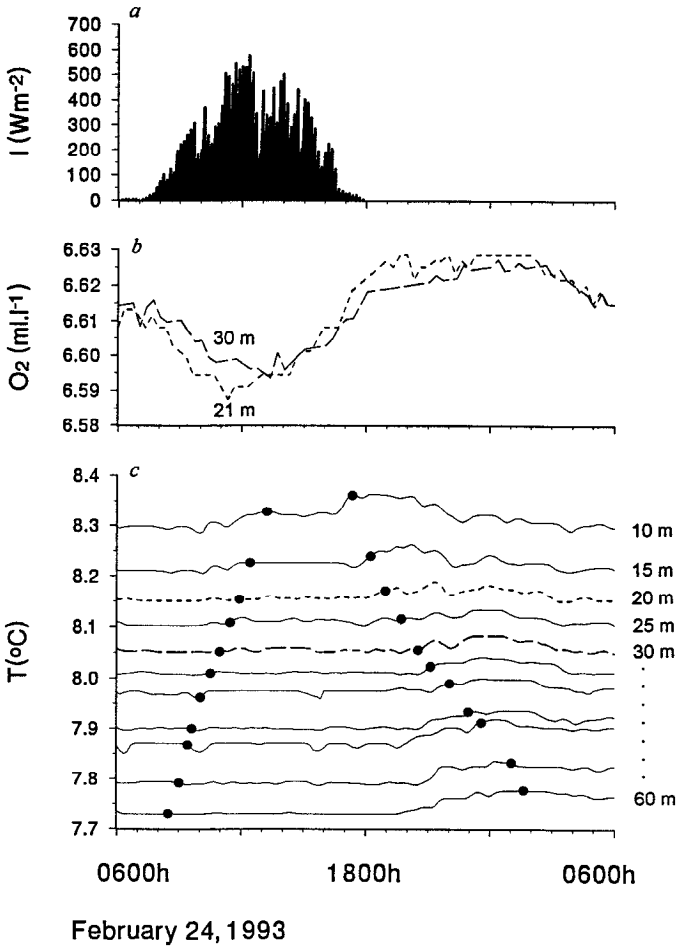

Figure 6. Measurements made from sunrise on 24 February to sunrise on 25 February of: (a) solar radiation intensity recorded by a ship mounted weather station; (b) dissolved oxygen at 21 m (-----), 30 m (———); and (c) water temperature recorded by the thermistor chain from 10 m to 60 m depth. Thermistors were separated by 5 m depth, and are shown with temperature offsets between adjacent thermistors of −0.05°C. The 20 m and 30 m records are highlighted in accordance with (b) above. The slight warming at depths > 40 m during the evening may be advective. Float penetration depths are also indicated (●) for comparison.

b. Development. The upper ocean mixing layer model is shown schematically in Figure 7, and includes a mixed layer of depth $h(t)$, mixed layer dissolved oxygen concentration $c(t)$, dissolved oxygen concentration below the mixed layer $c_d(t, z)$, biological production term $P(t, z)$, depth and time independent respiration term R, and surface gas flux $q(t)$. Here t denotes time and z depth. The mixed layer budget

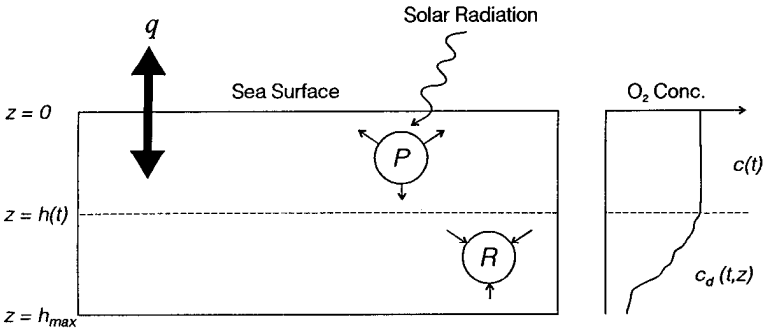

Figure 7. Schematic diagram of the model used to help interpret the data.

equation is:

$$h\frac{dc}{dt} = q - w_e(c - c_d|_{z=h}) + \int_{z=0}^{h} \{P(t,z) - R\}\, dz, \tag{1}$$

where:

$$w_e = \begin{cases} \dfrac{dh}{dt} & \text{if } w_e > 0 \\ 0 & \text{otherwise} \end{cases} \tag{2}$$

The dissolved oxygen concentration in a stratified layer of water below the mixed layer between depth $z_o - \Delta z/2$ and $z_o + \Delta z/2$ ($\Delta z \ll h$), is described by:

$$c_d(t_o + \Delta t, z_o) = c_d^o + \frac{\Delta t}{\Delta z}\int_{z_o-\Delta z/2}^{z_o+\Delta z/2} \{P(t_o, z_o) - R\}\, dz \tag{3}$$

where $c_d(t_o, z_o) = c_d^o$. In this model, vertical diffusion has been neglected. It is considered that the float trajectories will correctly indicate the penetration depth of the larger scale convecting plumes, but will not be influenced significantly by mixing scales of order or smaller than the instrument dimensions (~ 1 m). It is a limitation of our model that we use a two-layer representation of a mixing process that is observed to have a diffuse property gradient at its lower boundary. The implications of this approximation are discussed when comparing model and data results.

We shall suppose that light intensity, $\Theta(t, z)$, is attenuated exponentially with depth according to Beer's law:

$$\Theta(t,z) = I(t)e^{-kz} \tag{4}$$

where k is the vertical diffuse attenuation coefficient. Here $I(t)$ is the time dependence of the solar radiation intensity at the water surface, which we approximate in

accordance with Ikusima (1967) by;

$$I(t) = \begin{cases} 0 & \text{for } 0 \leq wt < \theta \\ I_o \sin^n (wt - \theta) & \text{for } \theta \leq wt \leq \pi \end{cases} \tag{5}$$

where n and θ are chosen to match the observations (this approximation is better for large n and small θ, as observed).

We choose to make new production, $P(t, z)$, proportional to the local solar light intensity[3], or:

$$P(t, z) = \delta k \Theta(t, z) \tag{6}$$

where δ is the production efficiency, having dimensions [mol $O_2 \cdot J^{-1}$]. As δ is defined to be constant, this introduces the assumption that the phytoplankton concentration is independent of depth and time. Phytoplankton reproduction, mortality and grazing will allow some depth-dependent phytoplankton stratification to build up during the day. However, vertical mixing each night will tend to reduce the importance of these effects. Both photo-inhibition and hysterisis in photosynthetic response are neglected for simplicity, although photoinhibition is most certainly a dominant process affecting the total oxygen production in the isolated surface layer (say < 10 m depth). The Lagrangian measurements could in principle be used to study the effect of hysterisis, however we are not attempting to model the dissolved oxygen concentration quantitatively. The production rate of oxygen per unit volume, daily averaged and vertically integrated over the maximum mixed layer depth, P_{avg}, is found to be:

$$\begin{aligned} P_{\text{avg}} &= \frac{w}{h_{\max}\pi} \int_{z=0}^{h_{\max}} \int_{t=0}^{\pi/w} P(z, t)\, dtdz \\ &= \frac{I_o \delta \Gamma_n}{h_{\max}\pi} (1 - e^{-kh_{\max}}) \end{aligned} \tag{7}$$

where $\Gamma_n = \int_{\tau=0}^{\pi} \sin^n \tau \, d\tau$.

Respiration is known to be a complicated function of depth and time. Phytoplankton and bacterial respiration are species- and environment-dependent; zooplankton grazing is complicated further by their mobility and photo-response (e.g., Frost, 1991). Subject to these approximations, we choose to simplify respiration in the model, R in Eq. (1), by expressing it as a depth-independent fraction F of the average production of oxygen in the water column, or:

$$R = FP_{\text{avg}}. \tag{8}$$

3. The vertical length scale associated with production at a depth z is k^{-1}.

c. Model inputs. A composite plot of the observed surface solar radiation intensity for the time period of interest is shown in Figure 5a. The envelope of this plot is used directly in the model with $n = 9$ (see Eq. 7) and hence $\Gamma_9 = 0.259$ (Abramowitz and Stegun, 1970). Fluorometer measurements taken at the experiment site (C. Wirick, Brookhaven National Laboratories, N.Y., personal communication) indicate a vertical diffuse attenuation coefficient for photosynthetically active radiation of $k \approx 0.1\ m^{-1}$. For these parameters the majority of oxygen production is confined to a relatively thin (~ 10 m) surface layer.

The surface gas flux is set to zero. This is justified as follows. From the diurnal oxygen increase observed at 30 m depth and surface gas flux obtained from transfer coefficients using historical data (Liss and Merlivat, 1986), we find that daily changes in the dissolved oxygen concentration are at least five times that expected from surface gas transfer alone. This can also be seen from the time series of inferred dissolved gaseous nitrogen (Fig. 1d). On time scales of a day, elemental di-nitrogen is essentially biologically inert. Therefore, the dissolved nitrogen concentration can change only by entrainment across the seasonal thermocline, advection and/or surface gas exchange. The CTD and thermistor chain data show minimal effects of advection or entrainment (significant advection occurred later in the experiment). The constant dissolved nitrogen concentration therefor implies that surface gas transfer is a small effect and of secondary importance in interpreting the oxygen time series.

We use the results of the neutrally buoyant mixed layer float to indicate the penetration depth of the mixing layer (dashed curve on Fig. 5c). We set $F = 1$ in Eq. 8. This is seen from Figure 1d where respiration approximately balances production over a day (this is true to within $\sim 13\%$, given that we have no measurements of horizontal fluxes). Setting $F = 1$ also allows a check of the model results with the analytical solution for the average oxygen production given by Eq. 7.

d. Model results. Appropriate scales used for nondimensionalization of the model results are: h_{max}—the maximum depth of the mixed layer in the model in meters; c^*—the mean mixed layer saturation concentration in $molO_2 \cdot m^{-3}$; T—time scale in days.

Figure 8a compares the mixed layer depth with the model results. Figure 8b shows the modelled solar radiation intensity as a function of depth, which is the solution of Eq. 4, and Figure 8c shows the water column dissolved oxygen concentration derived from the model. The model has been initialized with the vertical dissolved oxygen structure set from the previous day.

The model predicts a phase lag between the maximum in the near surface dissolved oxygen (approximately 1600 h) and the local solar radiation maximum near noon. Although we have no reliable time series of near-surface dissolved oxygen measurements, this same signature was observed in the thermistor chain record

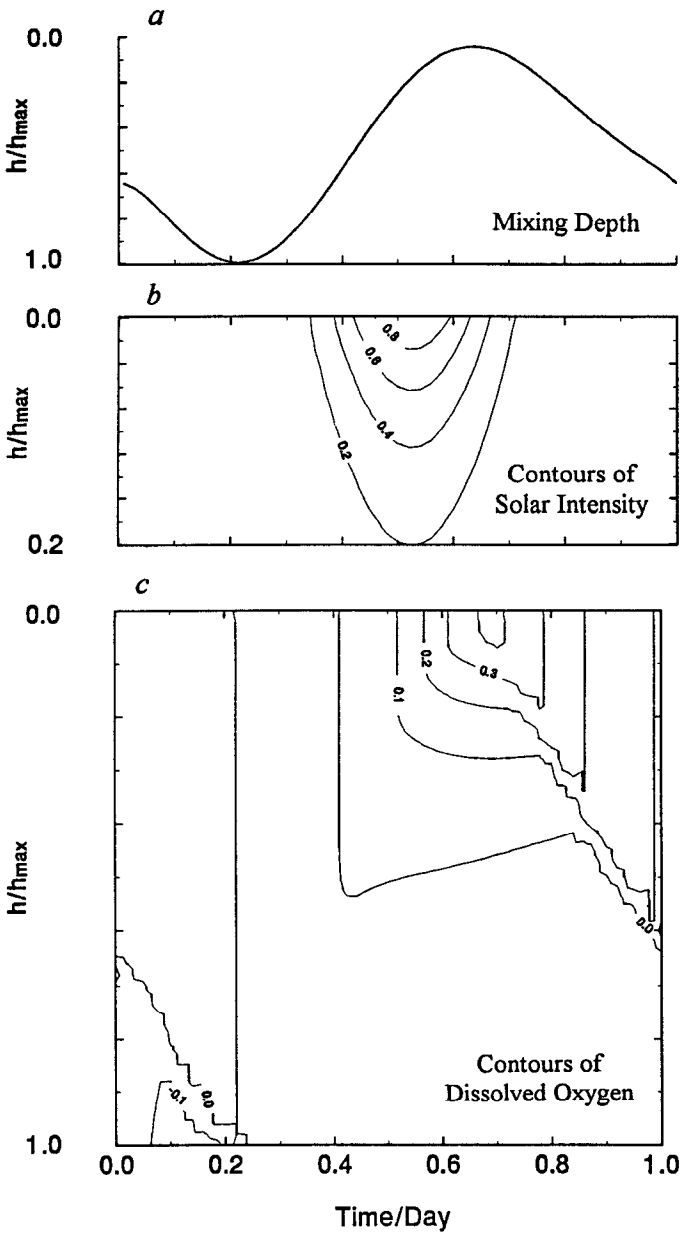

Figure 8. Model inputs and results, showing: (a) normalized model mixed layer depth, taken from the envelope of the neutrally buoyant float data (dashed line on Fig. 5c); (b) contour plot of modelled solar radiation intensity with time and depth (note the scale change on the depth axis); (c) contour plot of modelled dissolved oxygen percent saturation level for $F = 1$ in Eq. 8.

(Fig. 4) where the isolated surface layer temperature measured at 10 m depth has a maximum at 1600 h. This is a consequence of the fact that the heat content of the water is a time integral of the solar radiation absorbed during the day. As the short wavelength component of the solar radiation is driving oxygen production in the model, it is clear that this effect will also be apparent in the modelled dissolved oxygen concentration. Local respiration exceeds production below the oxygen compensation depth, which varies throughout the day. In the model, the dissolved oxygen content of the deeper waters continually decreases, and vertical dissolved oxygen gradients develop in the stratified water column below the mixed layer.

At the onset of convection, the warmer and more oxygenated surface water is mixed with the deeper, colder and less oxygenated water. With increasing sensor depth the oxygen maximum will occur at a later time as seen in the model results (Fig. 8c) and the data (Fig. 2b). Thermistor chain data (Fig. 4) show this effect for water temperature. Figure 9c shows time series of the model results at the near surface, and the two depths at which dissolved oxygen was measured. At 30 m the model predicts an oxygen maximum at approximately 2000 h, in agreement with the observations (Fig. 2c). The model also predicts a larger diurnal oxygen range for the deeper sensors, in accordance with the observations. Continued respiration occurs in the model throughout the day, decreasing the deeper water dissolved oxygen content.

4. Discussion

The model reproduces certain key features of the observations, particularly during periods of strong convection, and makes some predictions of the dissolved oxygen concentration in the rest of the water column throughout the day. Specifically, the model explains the diurnal oxygen variability as a consequence of the balance between surface production, convective mixing and respiration. The convective mixing is crucial to the redistribution of a thin surface production layer and explains the observed time delay in the oxygen maximum measured at progressively greater depths.

The simplifying assumptions used in the model development limit the extent to which quantitative predictions can be made. The most noticeable discrepancies between the model results and the data are the predicted instantaneous oxygen maximum at a given depth during the evening, coincident with the passage of the mixed layer past the sensor, and the timing of the oxygen minimum in the morning at the sensor depth, which is several hours earlier than the observations. These discrepancies can be explained by considering the effects, not included in the model, of smaller scale time and depth varying vertical mixing processes. Also, during the evening when the convective layer deepens beyond the measurement depth, the entraining dissolved oxygen concentration that has built up during the day will chiefly govern the oxygen time series recorded by a sensor. Oxygen stratification in the water

column is determined primarily by biological processes, particularly respiration. An inadequate description of these processes will be apparent in model and data comparisons.

The larger convective motions, which result from surface cooling, store kinetic energy that continues to be available for further mixing several hours after the buoyancy flux changes sign (Brainerd and Gregg, 1993). This can result in residual mixing below the shallow surface layer. As convection proceeds in the evening, energy is fed back into the larger scale motions, providing more energy for mixing and redistribution of the shallow surface layer temperature and dissolved oxygen anomaly. Thus a time and depth-dependent vertical mixing would be expected, with decreasing vertical gradients in temperature and dissolved oxygen as convection homogenizes the water column. As the turnover time scale for the larger convective motions is 2–4 h we do not expect complete homogenization of the water column until early the next morning. We shall now discuss what effects these processes would have in modifying the model results if they were included in a more comprehensive model, firstly for the restratification period then for the deepening period.

During the restratification period, at any given depth the dissolved oxygen concentration represents a consequence of the competing effects of both oxygen sources and sinks, the minimum occurring when they are equal in magnitude. The oxygen sources include local production, which is concentrated near the surface, and turbulent mixing down from the near-surface layer to the sensor depth. This vertical mixing is inhibited as the near surface warms. The oxygen sinks include local respiration and the mixing of the oxygen deficit resulting from respiration elsewhere in the water column. Our observations (Fig. 2b) show an oxygen minimum at 21 m occurring before the minimum at 30 m. This implies that the oxygen sources at 21 m at 1100 h exceed the oxygen sinks, whereas this balance does not occur at 30 m until about 1300 h. The timing of the minimum is not accurately predictable in our model, because the model does not include time and depth-dependent variations in the turbulent processes within the mixing layer.

During the evening a similar process occurs in reverse, except the surface buoyancy flux which previously restratified the surface water has now changed sign resulting in convective instability due to cooling. The oxygen balance at any given depth is now between respiration, vertical mixing from above and entrainment from below. Again, the intensity of mixing is neither uniform over the mixing layer nor time invariant, and vertical gradients will develop allowing continual supply of warmer and more oxygenated water to greater depths for an extended period. The model reproduces the progressive delay with respect to depth of the measured dissolved oxygen maximum. However, since the representation is strictly two-layer, a sudden change occurs as the mixed layer advances past any given depth. The observations show a continuous increase in temperature and oxygen over several hours (Fig. 6) as oxygen is continually mixed down from above. As the near surface

gradients diminish, respiration and entrainment dominate the oxygen balance and the concentration decreases.

The observations show a continuously increasing dissolved oxygen level at 21 m from approximately mid-day until 2400 h. This continuous increase represents a smooth transition between the two distinct regimes discussed above. By mid-day the oxygen sources at this depth are limited to primary production, although there may be a weak and decaying residual turbulent exchange. As evening approaches, primary production ceases and convective mixing of oxygen rich water from the surface becomes the new source. The persistent, but diminishing vertical dissolved oxygen gradient, which together with the depth-dependent mixing maintains the source term at intermediate depth, is not represented in the model. This explains the difference between the predicted discontinuity and the smooth transition that is observed. The effect of the depth and time-dependent mixing in smoothing out the transition is sketched with dashed lines in Figure 9c.

Diurnal oxygen variations have previously been used to calculate productivity (e.g., Oudot, 1989). The clear diurnal convection signal presented here motivates an analysis of its implications for similar productivity calculations based on the diurnal oxygen cycle. If we first neglect the cycle of convective mixing and assume instead that mixing is continuous and extends to a fixed depth, productivity is estimated as $q = h\beta\Delta s/\Delta t$. Parameters appropriate for the present study are $\Delta s = 0.6\%$ (Fig. 1d), $h = 80$ m, $\beta = 293$ mmol $\cdot$ m^{-3} (Weiss, 1970) leading to $q = 140$ mmol $\cdot$ m^{-2} $\cdot$ (½ day)$^{-1}$.

Next consider the effects of diurnal convection on an oxygen measurement made at half the maximum depth to which mixing extends. When the surface waters containing most of the photosynthetically produced oxygen at the end of the day mix to the instrument depth, the signal recorded by the instrument will show a daily oxygen peak to trough excursion that is twice that observed if the layer was thoroughly mixed all day. In fact, the enhancement by convection of the diurnal oxygen variation observed at a particular depth depends primarily on the ratio of maximum mixed layer depth to instrument depth. This enhancement is between three and four for our data. These effects may well be important in explaining the discrepancy between *in situ* and *in vitro* measurements referenced above. This simple enhancement will not be the only determining factor as production and respiration will vary with depth and time. The entrainment term in Eq. 1 will play a major role in determining the observed oxygen time series at a particular depth.

As seen above, the importance of determining mixed layer depth is crucial to budget calculations of the type presented here. However it is difficult to infer the instantaneous mixing depth from temperature and salinity observations alone. We observed warming of the near surface water by ~ 0.2°C over 4 m depth during the day (see Fig. 3). Even in the absence of heat loss, the even distribution of this heat input over a 100 m mixed layer will increase the water temperature by only 8 m°C. This is a small signal for most CTD instruments and is undetectable by our thermistor chains,

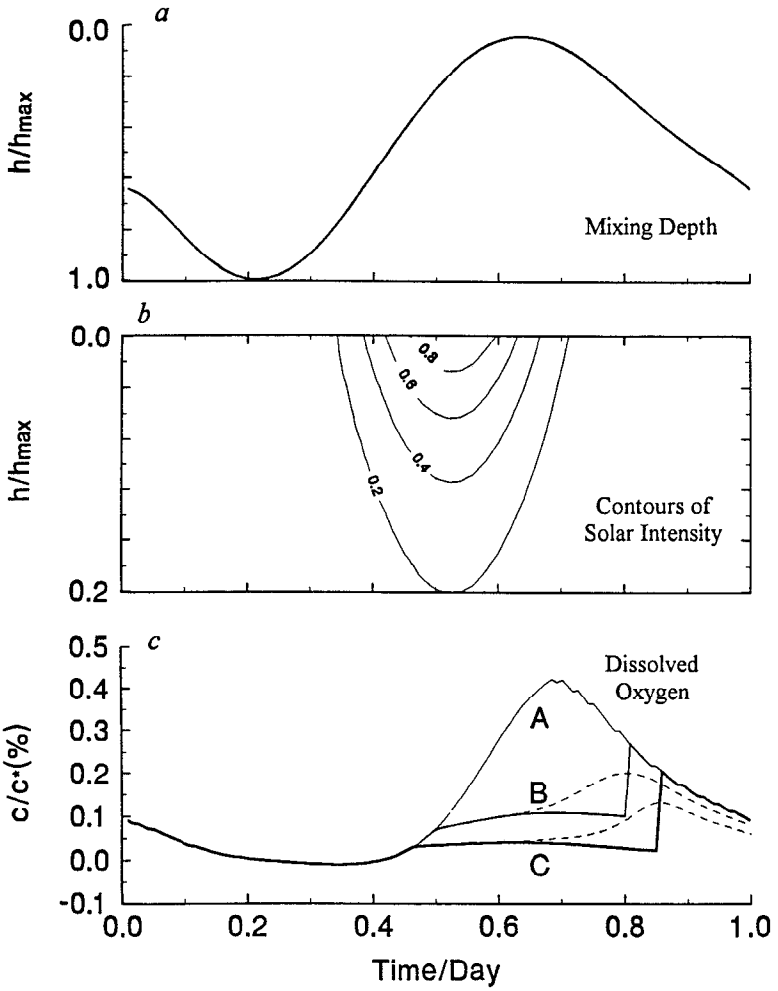

Figure 9. Model inputs and results, (a) and (b) are the same as in Figure 8. The model results at various depths are shown as solid lines in (c): A = surface, B = 20 m, C = 31 m. The dashed lines indicate what effect oceanic turbulence may have in smoothing out strong vertical gradients.

which have a resolution of 10 m°C. The use of neutrally buoyant float data or dissipation profiles (e.g., Brainerd and Gregg, 1993) provide more direct measurements of mixing layer depth which are essential for the interpretation of processes having time response comparable to or less than a day (c.f. Robertson *et al.*, 1993).

5. Conclusions

Our analysis has focused on the role of convection in redistributing photosynthetically produced dissolved oxygen. A correct interpretation of time series measurements at fixed depths depends upon the proper inclusion of convective mixing. This

conclusion applies not only to dissolved oxygen concentration, but to any biologically relevant scalar, like phytoplankton concentration (Gardner *et al.,* 1993) and organic/inorganic concentrations of photosynthetic products.

Although our simple mixed layer model identifies some essential features of the coupled physical-biological system, it cannot reproduce the consequences of the depth-dependent mixing intensity, or the role of photo-inhibition and hysterisis effects in photosynthetic response. These preliminary results provide motivation for a more comprehensive representation of the mixing layer and of the photosynthetic response and respiration, which is the focus of ongoing work.

Acknowledgments. The authors thank Bruce Johnson, Creighton Wirick, Doug Wallace, Ken Denman, Dave Mackas, Malgorzata Stramska and referees for comments and references. The thermistor chain data were processed by Tung Ho. We thank Geoffrey Dairiki and Eric D'Asaro (University of Washington, Seattle, USA) for kindly making available the mixed layer float data. This work was supported by NSERC under the Canadian JGOFS Program and by the US Office of Naval Research.

REFERENCES

Abramowitz, M. and A. Stegun. 1970. Handbook of Mathematical Functions. Dover, New York, 1046 pp.

Brainerd, K. E. and M. C. Gregg. 1993. Diurnal restratification and turbulence in the oceanic surface mixed layer—part I: Observations. J. Geophys. Res., *98,* 22645–22656.

Fahnenstiel, G. L. and H. J. Carrick. 1988. Primary production in lakes Huron and Michigan: *in vitro* and *in situ* comparisons. J. Plankton Res., *10,* 1273–1283.

Farmer, D. M., C. L. McNeil and B. D. Johnson. 1993. Evidence for the importance of bubbles in increasing air-sea gas flux. Nature, *361,* 620–623.

Frost, B. W. 1991. The role of grazing in nutrient-rich areas of the open sea. Limnol. Oceanogr., *36,* 1616–1630.

Gardner, W. D., I. D. Walsh and M. J. Richardson. 1993. Biophysical forcing of particle production and distribution during a spring bloom in the North Atlantic. Deep-Sea Res. II, *40,* 171–195.

Ikusima, I. 1967. Ecological studies on the productivity of aquatic plant communities. III. Effect of depth on daily photosynthesis in submerged macrophytes. Bot. Mag. Tokyo, *80,* 57–67.

Kennish, M. J. (ed.). 1989. Practical Handbook of Marine Science, C.R.C. Press, Inc., Boca Raton, Florida, 710 pp.

Liss, P. S. and L. Merlivat. 1986. Air-sea gas exchange rates: Introduction and synthesis, *in* The Role of Air-Sea Gas Exchange in Geochemical Cycling, P. Buat-Menard, ed., D. Reidel Pub. Co., Dordrecht, Holland, 113–127.

McNeil, C. L., B. D. Johnson and D. M. Farmer. 1994. *In situ* measurement of dissolved nitrogen and oxygen in the ocean. Deep-Sea Res., (in press).

Oudot, C. 1989. O_2 and CO_2 balances approach for estimating biological production in the mixed layer of the tropical Atlantic Ocean (Guinea Dome area). J. Mar. Res., *47,* 385–409.

Patterson, J. C. 1991. Modelling the effects of motion on primary production in the mixed layer of lakes. Aquatic Sciences, *53,* 218–238.

Robertson, J. E., A. J. Watson, C. Langdon, R. D. Ling and J. W. Wood. 1993. Diurnal variation in surface pCO_2 and O_2 at 60N, 20W in the North Atlantic. Deep-Sea Res. II, *40,* 409–422.

Stramska, M. and T. D. Dickey. 1993. Phytoplankton bloom and the vertical thermal structure of the upper ocean. J. Mar. Res., *51,* 819–842.

Taylor, A. H. and J. A. Stephens. 1993. Diurnal variations of convective mixing and the spring bloom of phytoplankton. Deep-Sea Res. II, *40,* 389–408.

Weiss, R. F. 1970. On the solubility of nitrogen, oxygen and argon in water and seawater. Deep-Sea Res., *17,* 721–735.

Wood, J. D. and R. Onken. 1982. Diurnal variation and primary production in the ocean—preliminary results of a Lagrangian ensemble model. J. Plankton Res., *4,* 735–756.

Received: *7 December, 1993;* revised: *7 July, 1994.*